STATISTICAL ANALYSIS OF BLAST WAVE DECAY COEFFICIENT AND MAXIMUM PRESSURE BASED ON EXPERIMENTAL RESULTS

SANJA LUKIĆ, HRVOJE DRAGANIĆ, GORAN GAZIĆ & IVAN RADIĆ
Faculty of Civil Engineering and Architecture Osijek, Josip Juraj Strossmayer University of Osijek, Croatia

ABSTRACT

Various expressions have been given in the literature for calculating blast wave parameters. Without experimental testing, it is difficult to determine which expression will predict the actual measurements more realistically. In this paper, a statistical analysis of two blast wave parameters, maximum overpressure and pressure-time diagram decay coefficient, was conducted based on field tests of the cylindrical TNT charge free-air detonation. Simple numerical simulation was also performed in order to compare the obtained maximum overpressures with the field test measurements. A comparison of the maximum free-field overpressures provided insights on the influence of the air mesh size as this proved to be a critical parameter. Statistically obtained blast wave decay coefficient and the maximum overpressure was compared with the analytical expressions given by different authors to determine the most appropriate description of experimental tests. Expressions are given depending on the scaled distance, i.e. the ratio of standoff distance to measuring sensors and cubic root of the charge mass. Expressions for blast wave parameters are used for a quick approximation of blast load for further analysis of structural elements, so their accurate determination ensures more realistic blast analysis and safer design.
Keywords: blast wave, pressure profile, decay coefficient, statistical analysis, free-air detonation.

1 INTRODUCTION

After the detonation of explosive material, the blast wave is generated. Blast wave travels to target through the air environment reaching its target and generating pressures on target surfaces. This is characterized by a sudden increase in pressure value. The arrival time (t_A) represents the time it takes for the shock wave front to arrive from the center of the detonated charge to the target. As the blast wave impinges its target and travels further into the environment, the pressure value is decreasing, even taking negative values, and eventually rises again to atmospheric pressure. The blast wave is usually represented as the pressure-time diagram described by several parameters.

Based on the above description, the blast pressure-time diagram can be divided into two parts, a positive and a negative phase. The positive phase is characterized by maximum positive pressure (p_{s0}) and duration of overpressure, i.e. duration of positive phase, t_0. The negative phase is characterized by negative pressure ($\bar{p}_{s0}$) and duration of under-pressure i.e. duration of negative phase, $\bar{t}_0$. A decrease in pressure value is represented by a wave decay coefficient (b). The blast wave decreases non-linearly and exponentially. Due to different nature of blast action, an additional parameter is used for blast load description and that is the impulse (i) of blast load which is defined as an area under the positive phase of the pressure-time diagram [1]. The parameters of blast wave can be seen in Fig. 1.

The negative phase is usually neglected to simplify the interpretation of blast load effects [2]. This is due to the negligible pressure value in comparison to that of the positive phase. Also, instruments for measuring blast pressure are designed to measure only positive overpressure. High temperatures and bright flash generated in explosion can influence pressure sensors and cause the recording of negative values. In our experiment, this is
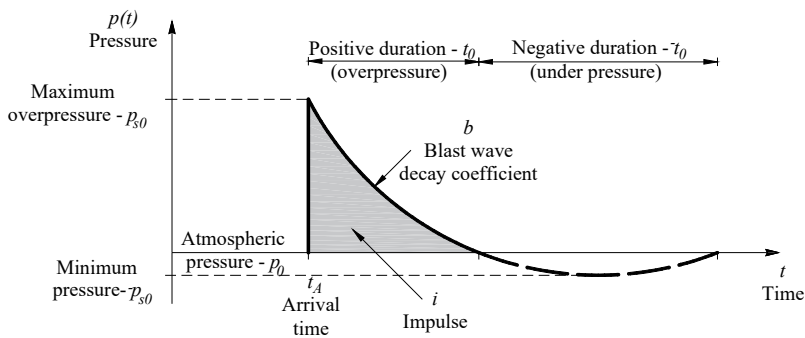
Figure 1: Ideal blast wave pressure-time diagram.

Figure 2: Experimentally measured blast wave.

mitigated by applying the adhesive tape over the sensing part of the sensor, but silicone grease can also be used. An actual, measured pressure-time diagram is shown in Fig. 2.

The Friedlander equation, eqn (1), is used to represent the change in pressure over time, $p_s(t)$, i.e. it provides a pressure-time diagram:

$$p_s(t) = p_{s0} \left(1 - \frac{t}{t_0} \right) \cdot e^{-\frac{b \cdot t}{t_0}}. \tag{1}$$

To determine the pressure-time diagram, it is necessary to know the maximum overpressure (p_{s0}), the blast wave decay coefficient (b), and the duration of the positive phase (t_0) [2]. Due to the lack of experimental testing, analytical expressions are used to determine these parameters. There are many various analytical expressions describing blast parameters, and it is difficult to select the most appropriate due to large discrepancies in the calculated values. The main reason for this is the dissimilarity of experimental tests used for expression derivation. There is no global consensus on experimental setup and procedures for determination of blast parameters. Due to these reasons comparison with statistically determined values was conducted to identify an appropriate expression. Maximum free-field (incident) overpressures obtained by field test and numerical simulations conducted in Ansys Autodyn software are compared with analytical expressions given in the literature. In addition to maximum free-field overpressures, the blast wave decay coefficients obtained by statistical analysis of experimental results are compared to analytical predictions.

<div align="center">2 OUTLINE OF EXPERIMENT</div>

Field experiments were conceived to determine the two blast wave parameters, that is, the blast wave decay coefficient and the maximum free-field overpressure, and to compare them with analytical values obtained from the literature.

2.1 Description of explosives

Lead azide detonator capsules were used for initiating explosive reaction of a TNT charge as secondary (high) explosive [1]. Lead azide is a primary explosive, with strong brisance (fragmentation) properties. It is widely used in detonator manufacturing because it has a stable shelf life. However, it is extremely sensitive to stray ignition sources (including electrostatic discharge) and becomes shock-sensitive if it is crystallized. The shape of the TNT (trinitrotoluene, trotyl) charge is a cylinder with a height of 100 mm and a base radius of 30 mm. 100 g of explosives were detonated at each measurement. Charge geometry and detonator capsules are shown in Fig. 3. The experiment was conducted in cooperation with the Croatian Police, Anti-Explosion Service Osijek at their training ground.
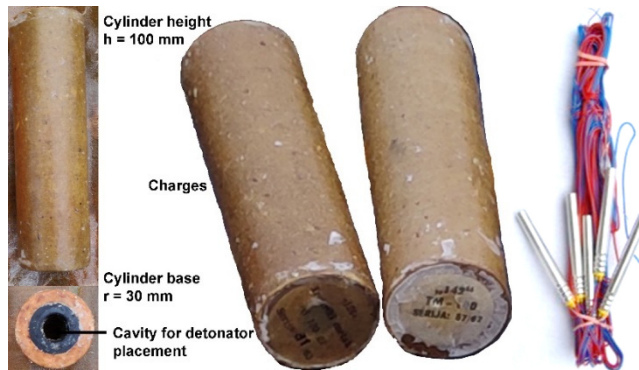

<div align="center">Figure 3: Charge geometry and detonator capsules filled with lead azide.</div>

2.2 Experimental set-up

The field tests consisted of detonating a predetermined quantity of explosives (100 g of TNT) at a certain distance from pressure sensors. The pressure sensor distance was increased through each subsequent detonation to determine the trend of the pressure regarding the distance change from the detonation point (standoff distance). The explosion wave pressure in free air (incident overpressure) was measured. Four quartz free-field ICP® blast pressure pencil probes were used to measure incident overpressures. Pencil probes were placed at an equal distance from the centre of the TNT charge as can be seen in Fig. 4. Pencil probes were designated as 11126, 11127, 11128 and 11129. The longitudinal axis of the cylindrical charge was directed to sensor 11128, as a front sensor. Sensors 11126 and 11127 are the lateral sensors, located perpendicular to cylindrical TNT charge and 11129 is the rear sensor. The instrumentation should have as little deviation as possible from the longitudinal and perpendicular burst of the blast wave. The charge was placed on a wooden stand at a height of 1.0 m in all tests. The sensors were placed at the same height and were directed at the charge. The positions of pencil probes are shown in Fig. 5(a). Three detonations were made at each distance to obtain a larger data set of measured pressures for comparison and

statistical analysis. The detonations were performed at seven different standoff distances, shown in Table 1. The weight of the explosive is labelled as W, the actual distance from the centre of the explosive to the sensor (standoff distance) as R, and the scaled distance as Z. The position of the sensors at a distance of 0.743 m ($Z = 1.6$ m/kg$^{1/3}$) was proved to be too close to the blast, and the sensors were caught in the fireball. Blast fireball is a phenomenon where explosive material is burnt in the air while expanding from its origin of detonation. If measuring sensors are located in the vicinity of the charge blast fireball, pressure data can be corrupted, resulting in unrealistic pressure and impulse values. Fireball high temperatures and bright flash influences sensors by disrupting their inner workings through sensor casing deformation, sensor overheating and vibration. Fig. 5(b) shows blast fireball engulfing the pressure probes.
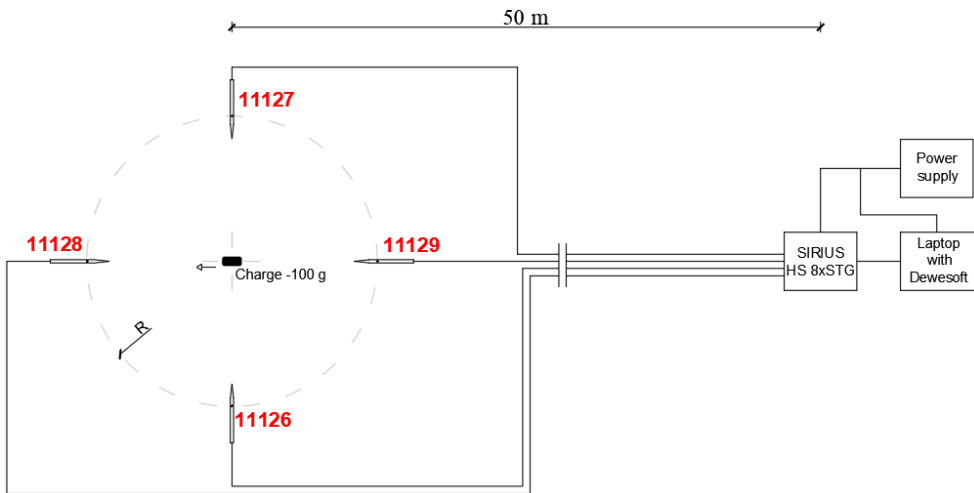

Figure 4: Scheme of experimental set-up.

(a)   (b)

Figure 5:   (a) Position of the instruments on the test site; and (b) and blast fireball after detonation.

Table 1: Field test parameters.

Field test	1	2	3	4	5	6	7
W (kg)	0.1	0.1	0.1	0.1	0.1	0.1	0.1
R (m)	0.743	0.835	0.928	1.160	1.392	1.625	1.857
Z (m/kg$^{1/3}$)	1.60	1.80	2.00	2.50	3.00	3.50	4.00
No. of detonations	3	3	3	3	3	3	3

3 NUMERICAL MODELLING OF EXPERIMENTAL MEASUREMENTS

Numerical simulation of blast pressure field tests was conducted in Ansys Autodyn software [3]. An experimental setup was modelled using 2D axial symmetry Multi-material Euler Godunov solver [4]. Symmetry was incorporated into the model for faster calculation. The model consisted of two parts, air and explosive material. Air was modelled as an ideal gas with atmospheric pressure initializing at the start of the simulation while explosive was modelled as TNT, via Jones–Wilkins–Lee (JWL) equation of state [5], [6]. Air is a gaseous material and as such, there is no possibility of stress transfer. Thus, the air is not influenced by any change of strength or failure principles and serves solely as a medium that transfers blast/impact waves generated by detonation. Similar to air, explosive material does not have any strength, nor is it susceptible to failure, but it is essential for generating blast waves. Material characteristics of air and TNT charge can be found in Autodyn material library.

Field tests were conducted using a cylindrical TNT charge. The geometry of charge is shown in Fig. 3. Based on charge weight, the radius of the cylinder base and its height was determined and compared with the charge used in the experiment. The charge weight was considered as a constant value throughout all field tests, so the cylinder base and height were unknowns for modelling real mass of explosive. After considering all possibilities, it was decided to fix the radius of the base and to determine the height based on those two values, cylinder mass and base radius. The cylinder base radius was selected as the radius measured on charges used in field tests with a value of r = 30 mm. Furthermore, the height of the cylinder was derived from the simple mass equation with value h = 87 mm. This is somewhat smaller than the actual height of the charge, which is approximately 100 mm, but this is because the actual charge is partially hollow. The cavity is intended to place the detonator and initiate an explosion.

Based on the performed verification, the same geometry and mass of the charge was entered in the numerical model. The only difference between the numerical model of the charge and charge used in field tests is that the real charge was encased in a thin paper mould to maintain its geometry during the storage time. This was considered to have a negligible influence on charge blast energy release, i.e. this could not provide sufficient rigid confinement to enhance blast intensity. For this reason, the paper mould was not modelled in numerical simulations. The point of blast initiation, i.e. charge detonator was assumed to be at the centre of a cylindrical charge, considering both axes. The x and y axes are the axial and radial directions, respectively. Four air mesh element sizes (2.5, 5, 10 and 20 mm) were used for numerical simulations to study the influence of air mesh size on blast pressures. Based on performed simulations, all air mesh sizes give approximately equal maximum free-field overpressures. To reduce computational time but maintain accuracy, 5 mm air mesh size was selected as a referent for further analysis. The charge air environment volume was considered in such a way as to include all charge to gauge point distances. This was possible because, in the numerical model, gauge points are fictive objects placed in the air environment. If the points are fictive and located one in front of another, they do not generate drag and influence

overall pressure value and shape. In the field tests, the distance of the pencil probes was adjusted from test to test. Numerically obtained incident pressures were measured by gauge points located at the same distances as pencil probes. At the edge of the air domain, flow-out boundary condition was assigned to avoid blast pressure wave reflection and disruption of blast pressure measurements. Fig. 6 shows a numerical model of the experimental measurements.
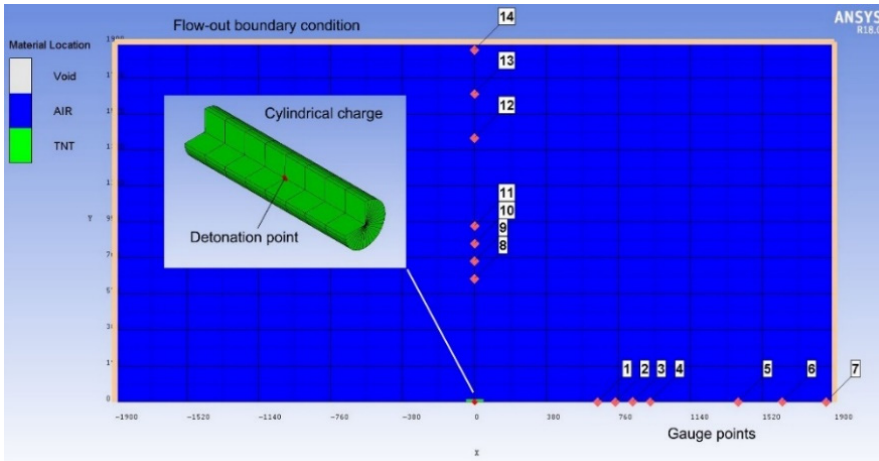

Figure 6: Numerical model.

4 EMPIRICAL AND ANALYTICAL EXPRESSIONS

4.1 Maximum free-field (incident) overpressure

There are various analytical expressions from different authors for calculating the parameters of a blast wave based on empirical or semi-empirical approaches [7]. Expressions for maximum incident overpressure calculation were used based on the assumption that explosive detonation is in free air and that the blast wave propagates spherically. Table 2 gives a list of authors and expressions considered in this study. Expressions for overpressure calculation depend on scaled distance (Z), which is the ratio of standoff distance (R) and the cubic root of the charge weight (W), or on weight and distance ratio specified by each author.

4.2 Blast wave decay coefficient

The blast wave decay coefficient (b) is a dimensionless coefficient that depends on the scaled distance (Z). The b is the most important coefficient for the determination of the blast load impulse. Impulse is important for design purpose because it refers to the total force (per unit area) applied on a structure due to the blast load [8]. The decay coefficient can be calculated iteratively using the Friedlander equation if the maximum overpressure, the duration of the positive phase and the impulse are known from the field tests. Ullah et al. [7], Karlos et al. [9] and Goel et al. [2] provide a list of the expressions of various authors for decay coefficient, the most commonly used are shown in Table 3. They show that at small-scaled distances ($Z < 2.0$ m/kg$^{1/3}$) the differences in the coefficient are significant [2], [7], [9].

Table 2: Maximum free-field overpressure (p_{s0}) according to different authors.

Authors	Pressure (MPa)	
Sadovskiy [10]	$$p_{\text{so}} = \frac{0.085}{Z} + \frac{0.3}{Z^2} + \frac{0.82}{Z^3}$$	(2)
Brode [11]	$$p_{\text{so}} = \frac{0.67}{Z^3} + 0.1$$	(3)
Naumyenko and Petrovskyi [12]	$$p_{\text{so}} = \frac{0.0745}{Z} + \frac{0.250}{Z^2} + \frac{0.637}{Z^3}$$	(4)
Adushkin and Korotkov [13]	$$p_{\text{so}} = \frac{0.08}{Z} + \frac{0.28}{Z^2} - \frac{0.322}{Z^3}$$	(5)
Henrych and Major [14]	$$p_{\text{so}} = \frac{0.0649}{Z} + \frac{0.397}{Z^2} + \frac{0.322}{Z^3}$$	(6)
Held [15]	$$p_{\text{so}} = 2\frac{W^{\frac{2}{3}}}{R^2}$$	(7)
Kinney and Graham [16]	$$p_{\text{so}} = p_0 \frac{808[1 + (\frac{Z}{4.5})^2]}{\sqrt{[1 + (\frac{Z}{0.048})^2]} \cdot \sqrt{[1 + (\frac{Z}{0.32})^2]} \cdot \sqrt{[1 + (\frac{Z}{1.35})^2]}}$$	(8)
Mills [17]	$$p_{\text{so}} = \frac{1.772}{Z^3} - \frac{0.114}{Z^2} + \frac{0.108}{Z}$$	(9)
Hopkins-Brown and Bailey [18]	$$p_{\text{so}} = \frac{0.0707}{Z} + \frac{0.3602}{Z^2} + \frac{0.4891}{Z^3}$$	(10)
Gelfand and Silnikov [19]	$$p_{\text{so}} = 1.7 \cdot 10^3 \exp(-7.5 \cdot Z^{0.28})$$	(11)
Bajić [20]	$$p_{\text{so}} = 0.102\frac{W^{\frac{1}{3}}}{R} + 0.436\frac{W^{\frac{2}{3}}}{R^2} + 1.4\frac{W}{R^3}$$	(12)
Li and Ma [21]	$$p_{\text{so}} = 0.084\frac{W^{\frac{1}{3}}}{R} + 0.27\frac{W^{\frac{2}{3}}}{R^2} + 0.7\frac{W}{R^3}$$	(13)

Table 3: Blast wave decay coefficient [2], [7], [9].

Authors	Blast wave decay	
Dharaneepathy [22]	$b = 3.18 \cdot Z^{-0.58}$	(14)
Lam et al. [23]	$b = Z^2 - 3.7 \cdot Z + 4.2$	(15)
Larcher [24]	$b = 5.2777 \cdot Z^{-1.1975}$	(16)
Teich and Gebbeken [25]	$b = 1.5 \cdot Z^{-0.38}$	(17)

5 RESULTS AND DISCUSSION

5.1 Free-field overpressure comparison

The maximum free-field overpressures measured with pencil probes (11126, 11127, 11128 and 11129) were extracted and compared to the pressures obtained numerically and analytically. Comparing the maximum free-field overpressures obtained by field tests, Figs 7 and 8 show that higher overpressures are obtained on sensors placed perpendicular to the direction of detonation (11126 and 11127). This observation is in accordance with [26]. After analysing videos of charge detonations, it was observed that the pencil probes located closest to the explosion ($Z = 1.6$ m/kg$^{1/3}$) were engulfed in blast fireball. As stated before, the fireball can cause data disruption which was noticed in measured overpressures. Due to this phenomenon, the difference in measured overpressures between sensors 11126 and 11127 at a scaled distance of 1.6 m/kg$^{1/3}$ is 95 kPa, which is 20%. At all other scaled distances, the differences between the measured overpressures are less than 20% which is considered acceptable, as can be seen in Fig. 7. Also, the obtained pressure distribution diagrams in time for these pencil probes correspond to the ideal shape of the blast wave. There is a significant difference in overpressures between the sensor 11128 to which the explosive is directed and sensor 11129 located directly behind, especially at smaller-scaled distances (1.6, 1.8, 2.0 m/kg$^{1/3}$). These differences are between 32% and 66%. It is assumed that one of the reasons is the position of the detonator and overall shape of the charge. At larger scaled distances (3.0, 3.5, 4.0 m/kg$^{1/3}$) as the distance increases deviations in measured overpressures between sensors 11128 and 11129 decrease from 15% to 1.5%, as can be seen in Fig. 8. The charge, as stated before, is partly hollow and that cavity is directed to sensor 11129. The purpose of the cavity is to place the detonator inside explosive material without additional interventions in the form of drilling or mechanical action that can accidentally trigger the explosion.
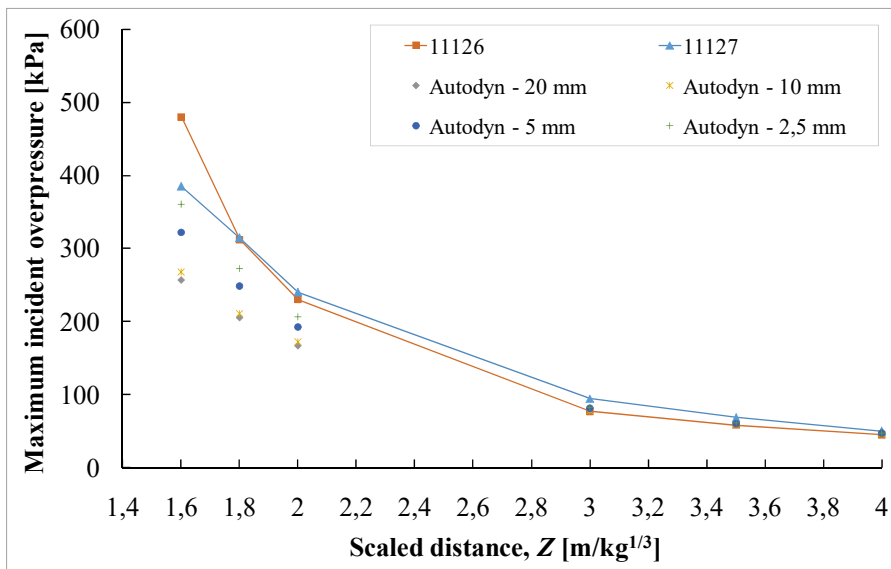

Figure 7:   Comparison of the measured pressure (pencil probes 11126 and 11127) and the pressure obtained in the numerical model (gauges 8, 9, 10, 11, 12, 13, 14).
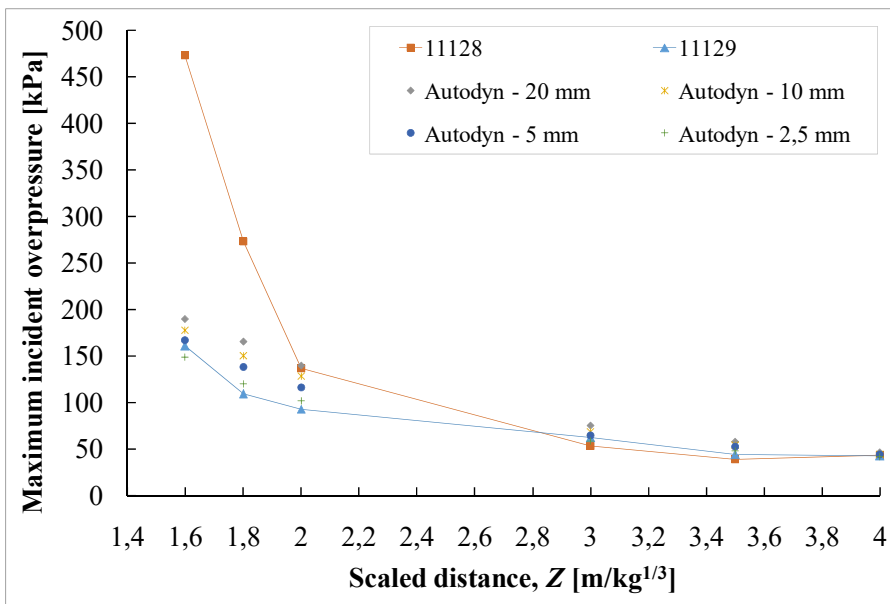
Figure 8:   Comparison of the measured pressure (pencil probes 11128 and 11129) and the pressure obtained in the numerical model (gauges 1, 2, 3, 4, 5, 6, 7).

Four numerical models were made in Autodyn, with the element size of the air mesh varied (2.5, 5, 10 and 20 mm) to compare the measured and numerically obtained overpressures. Similarly to the field tests, the numerical simulations gave higher lateral overpressures, i.e. overpressures perpendicular to the direction of charge. Larger differences between measured and numerically obtained overpressures from 10% to 46% occur at smaller scaled distances (1.6, 1.8, 2.0 m/kg$^{1/3}$), while at larger scaled distances (3.0, 3.5, 4.0 m/kg$^{1/3}$) the overpressures become almost equal regardless of the air mesh size and differences are between 0.05% and 18%. Compared to field test measurements at small-scale distances (1.6, 1.8, 2.0 m/kg$^{1/3}$) and for 2.5 mm mesh size, simulations give the closest overpressures to the measured values (differences vary from 6% to 25%), while at larger scaled distances (3.0, 3.5, 4.0 m/kg$^{1/3}$) they almost coincide (differences vary from 4% to 12%), so the mesh size, in this case, does not play a significant role, as can be seen in Fig. 7. Considering overpressures in the direction of the charge, it is interesting to note that the highest overpressures obtained are for the 20 mm mesh size while the lowest overpressures are obtained for 2.5 mm mesh size. Compared to the field test, numerically obtained maximum free-field overpressures are in better agreement with the values obtained by sensor 11129. The best coincidence is obtained for the densest mesh (2.5 mm), differences in pressure are from 1% to 10% compared to sensor 11129, and from 3% to 69% compared to sensor 11128, as can be seen in Fig. 8, although in this case, these are the lowest values.

Due to smaller values and inconsistencies in values as a result of the charge orientation, overpressures obtained with sensors 11128 and 11129 were not analysed in more detail. Only overpressures from sensors 11126 and 11127 were further analysed. According to expressions in Table 2, Held [15] and Bajić [20] overestimate maximum free-field overpressures measured by sensors 11126 and 11127 from 20% to almost 190% depending on the scaled distance, while Adushkin and Korotkov [13] underestimate overpressures from

70% to 83% at small-scaled distances (Fig. 9). Maximum overpressures obtained by expressions have larger deviations at smaller distances (1.6, 1.8, 2.0 m/kg$^{1/3}$), and are more uniform over larger scaled distances (3.0, 3.5, 4.0 m/kg$^{1/3}$). Expressions provided by Kinney and Graham [16] and Mills [17] give pressures that vary from 0.5% to 15% from those measured by sensors 11126 and 11127.
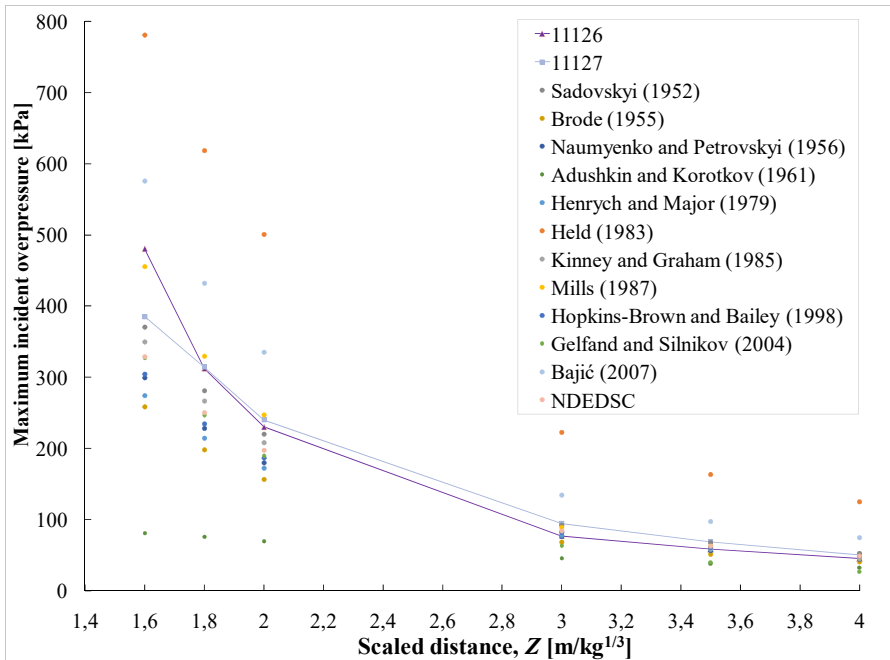

Figure 9: Comparison of pressures obtained analytically and experimentally.

5.2 Blast wave decay coefficient comparison

Pressure variation over time measured in the experiment is shown in Fig. 10 as discrete values (circles). These pressure values are obtained in the field test measurements. From each field test, maximum overpressure and positive phase duration were determined as input parameters for Friedlander equation, eqn (1). Using eqn (1), the pressure curve is fitted to the measured data (Fig. 10). Based on the fitted curve, the decay coefficient was determined. The decay coefficient b was obtained for all field tests using the Friedlander equation utilizing the nonlinear estimation and least-squares method in software Statistica [27], as given by Fig. 10. Due to discrepancies in the measurements and the observed inconsistencies in pressure-time diagrams for sensors 11128 and 11129, these results are not analysed in this section. All obtained values of coefficient b for measured data from pencil probes 11126 and 11127 are plotted versus distance Z in Fig. 11. The data obtained is best described by an exponential function. The exponential function is determined by estimating variables that best describe the given field tests.
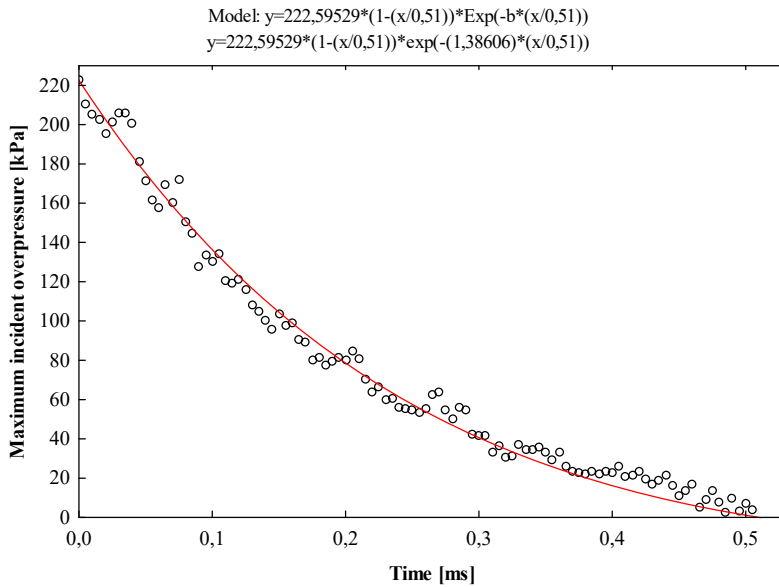
Model: y=222,59529*(1-(x/0,51))*Exp(-b*(x/0,51))
y=222,59529*(1-(x/0,51))*exp(-(1,38606)*(x/0,51))

Figure 10: Shape of the measured blast wave and fitted curve based on the Friedlander equation (sensor 11126, W = 0.100 kg, R = 0.928 m).
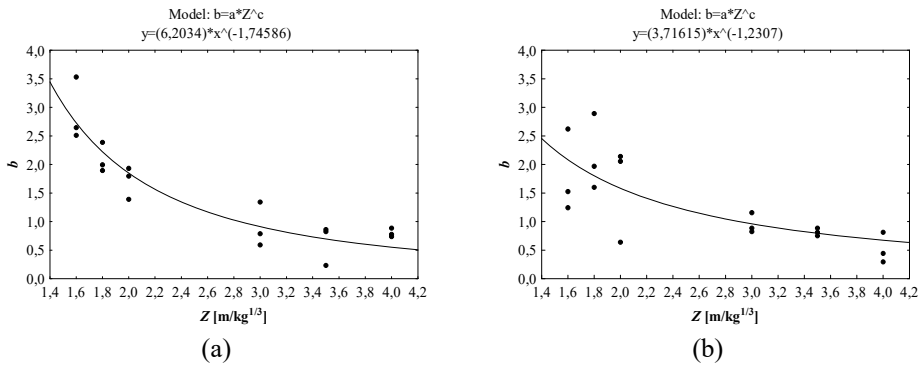

Figure 11: Variation of wave decay coefficient (b) with scaled distance (Z) measured by (a) Sensor 11126; and (b) Sensor 11127.

Variables for determining the upper and lower confidence limits were also obtained and are shown in Table 4. When comparing the expressions given in Table 3, with the obtained confidence intervals, for our field tests in Table 4, Larcher [24] with his expression best describes our results. The reason may be due to the large range between the lower and upper limits of the confidence interval. The width of the confidence interval depends on the sample size and the variation of data values. To obtain a more accurate model with a smaller confidence interval, it is necessary to increase the number of measurements and discard outliers in measurements.

Table 4: Estimation of models and parameters for calculating blast wave decay coefficient (*b*) with software Statistica.

Pencil probe	Model	Estimate	Lower conf. limit	Upper conf. limit
11126	$b = a \cdot Z^c$	a = 6.2034	4.25740	8.14941
	$y = 6.2034 \cdot x^{-1.74586}$	c = −1.74586	−2.22923	−1.26248
11127	$b = a \cdot Z^c$	a = 3.71615	1.84303	5.589270
	$y = 3.71615 \cdot x^{-1.2307}$	c = −1.23070	−1.93118	−0.530220

Fig. 12 shows curves obtained by expressions given by authors listed in Table 3 and fit curves from field tests obtained on pencil probes 11126 and 11127. The expression given by Lam et al. [23] does not describe experimental results well, especially, for differences seen at scaled distances greater than 3.0 m/kg$^{1/3}$, where the wave decay coefficient values are overestimated by a factor ranging from 2 to almost 9 times. Also, at a scaled distance for up to 2.0 m/kg$^{1/3}$, there is a good agreement with Dharaneepathy [22], the respective difference is from 1% to 35%, beyond that, there is a significant difference from 75% to 158%. The shape of the curve and the change in the coefficient *b* with scaled distance most closely coincides with the curve obtained through the Larcher [24] expression. When calculating decay coefficient *b* for each field test, the best agreement is with Teich and Gebbeken [25].
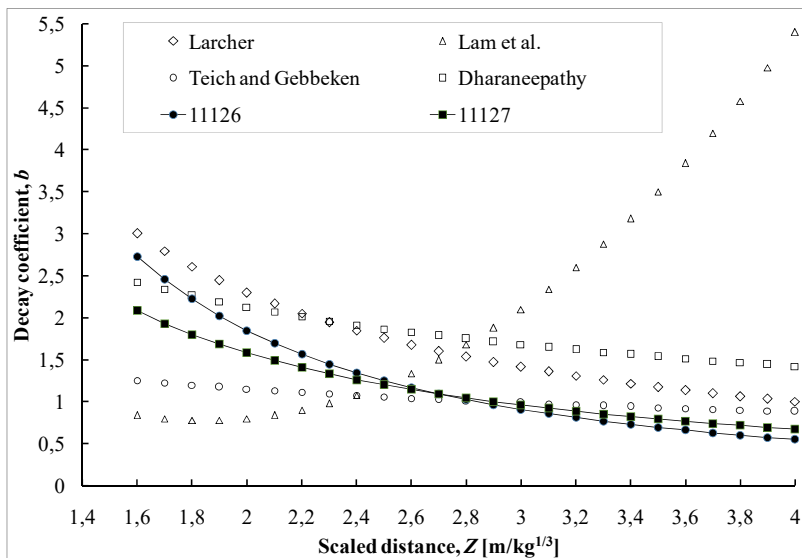

Figure 12: Variation of wave decay coefficient (*b*) with scaled distance (*Z*).

6 CONCLUSION

Performed field tests point out that the charge orientation has played an important role in terms of measured overpressures. Higher values were measured at the sensors placed perpendicular to the detonation direction (11126 and 11127). Due to blast fireball, the difference in measured maximum overpressures between sensors 11126 and 11127 at a scaled

distance of 1.6 m/kg$^{1/3}$ is significant. At all other scaled distances, the differences between the measured pressures are less than 20% of what is considered acceptable. Pressure values measured at sensors in the longitudinal direction (11128 and 11129) were significantly different at smaller scaled distances (1.6, 1.8, 2.0 m/kg$^{1/3}$), and it is assumed that these differences were caused by the position of detonator and overall shape of the charge. After comparing the measured and calculated maximum overpressures, the most approximate results are obtained by the Kinney and Graham [16] and Mills [17] expressions. At small-scale distances and with a 2.5 mm mesh size, simulations in Autodyn give the closest overpressures to the measured values. To reduce computational time but maintain accuracy, 5 mm mesh size can be selected as a referent for further analysis. As the scaled distance increases, a larger mesh size produces sufficiently accurate results. When analyzing the coefficient b for individual measurements, the results in the experiment most closely match the coefficient obtained by the Teich and Gebbeken [25] expression. Also, at a scaled distance for up to 2.0 m/kg$^{1/3}$, there is a good agreement with Dharaneepathy [22], beyond that, there is a significant difference.

REFERENCES

[1]   Ngo, T. et al., Blast loading and blast effects on structures: An overview. *Electronic Journal of Structural Engineering*, **7**(S1), pp. 76–91, 2007.

[2]   Goel, M.D. et al., An abridged review of blast wave parameters. *Defence Science Journal*, **62**(5), pp. 300–306, 2012.

[3]   ANSYS, *ANSYS AUTODYN User manual*, *ANSYS Release 14.0*. Canonsburg, PA, USA, pp. 1–464, 2010.

[4]   Kohnke, P., *ANSYS Theory Manual, Release 12.0*, ANSYS Inc., p. 1126, 2009.

[5]   Draganić, H. & Varevac, D., Numerical simulation of effect of explosive action on overpasses. *Građevinar*, **69**(6), pp. 437–451, 2017.

[6]   Draganić, H. & Varevac, D., Analysis of blast wave parameters depending on air mesh size. *Shock and Vibration*, **2018**, 3157457, 2018.

[7]   Ullah, A. et al., Review of analytical and empirical estimations for incident blast pressure. *KSCE Journal of Civil Engineering*, **21**(6), pp. 2211–2225, 2017.

[8]   Karlos, V. & Solomos, G., Calculation of blast loads for application to structural components. Report EUR, **26456**, 2013.

[9]   Karlos, V., Solomos, G. & Larcher, M., Analysis of the blast wave decay coefficient using the Kingery–Bulmash data. *International Journal of Protective Structures*, **7**(3), pp. 409–429, 2016.

[10] Sadovskiy, M.A., *Mechanical Effects of Air Shock Waves from Explosions According to Experiments, Selected Works: Geophysics and Physics of Explosion*, Nauka Press: Moscow, 2004.

[11] Brode, H.L., Numerical solutions of spherical blast waves. *Journal of Applied Physics*, **26**(6), pp. 766–775, 1955.

[12] Naumyenko, I. & Petroskyi, I., The shock wave of a nuclear explosion. BOEH, CCCP, 1956.

[13] Adushkin, V.V. & Korotkov, A.I., Parameters of a shock wave near to HE charge at explosion in air. *PMTF*, **5**, pp. 119–123, 1961.

[14] Henrych, J. & Major, R., *The Dynamics of Explosion and its Use,* Elsevier: Amsterdam, 1979.

[15] Held, M., Blast waves in free air. *Propellants, Explosives, Pyrotechnics*, **8**(1), pp. 1–7, 1983.

[16] Kinney, G.F. & Graham, K.J., *Explosive Shocks in Air*, Springer-Verlag: Berlin and New York, 1985.

[17] Mills, C.A., The design of concrete structure to resist explosions and weapon effects. *Proceedings of the 1st International Conference on Concrete for Hazard Protections*, pp. 61–73, 1987.

[18] Hopkins-Brown, M.A. & Bailey, A., Explosion effects, Part 1, AASTP-4, Royal Military College of Science, Cranfield University, 1998.

[19] Gelfand, B. & Silnikov, M., *Blast Effects Caused by Explosions*, European Research Office: London, 2004.

[20] Bajić, Z., Determination of TNT equivalent for various explosives. Master's thesis, University of Belgrade, Belgrade, Serbia, 2007.

[21] Li, J. & Ma, S., *Explosion Mechanics*, Science Press: Beijing, 1992.

[22] Dharaneepathy, M., Air blast effects on shell structures. PhD thesis, Anna University, Madras, 1993.

[23] Lam, N., Mendis, P. & Ngo, T., Response spectrum solutions for blast loading. *Electronic Journal of Structural Engineering*, **4**(4), pp. 28–44, 2004.

[24] Larcher, M., *Pressure-Time Functions for the Description of Air Blast Waves*, JRC Technical Note, 46829, 2008.

[25] Teich, M. & Gebbeken, N., The influence of the under pressure phase on the dynamic response of structures subjected to blast loads. *International Journal of Protective Structures*, **1**(2), pp. 219–234, 2010.

[26] US DoD, *UFC 3-340-02: Structures to Resist the Effects of Accidental Explosions,* US DoD: Washington, DC, USA, 2008.

[27] Statistica (data analysis software system), version 13, 2017.